Microbubble detection with adaptive beamforming for Ultrasound Localization Microscopy

Alexandre Corazza, Pauline Muleki-Seya, Abderrahmane Walid Aissani, Olivier Couture, Adrian Basarab, Barbara Nicolas

Microbubble detection with adaptive beamforming for Ultrasound Localization Microscopy

Alexandre Corazza
CREATIS UMR 5220, U1206
Univ Lyon, INSA-Lyon,
Université Claude Bernard Lyon 1,
UJM-Saint Etienne, CNRS, Inserm
F-69100, Villeurbanne, France
Alexandre.Corazza@creatis.insa-lyon.fr

Pauline Muleki-Seya
CREATIS UMR 5220, U1206
Univ Lyon, INSA-Lyon,
Université Claude Bernard Lyon 1,
UJM-Saint Etienne, CNRS, Inserm
F-69100, Villeurbanne, France
Pauline.Muleki@creatis.insa-lyon.fr

Abderrahmane Walid Aissani
Laboratoire d'Imagerie Biomédicale
Sorbonne Université, CNRS, INSERM
Paris, France
Walid.Aissani@sorbonne-universite.fr

Olivier Couture
Laboratoire d'Imagerie Biomédicale
Sorbonne Université, CNRS, INSERM
Paris, France
Olivier.Couture@sorbonne-universite.fr

Adrian Basarab
CREATIS UMR 5220, U1206
Univ Lyon, INSA-Lyon,
Université Claude Bernard Lyon 1,
UJM-Saint Etienne, CNRS, Inserm
F-69100, Villeurbanne, France
Adrian.Basarab@creatis.insa-lyon.fr

Barbara Nicolas
CREATIS UMR 5220, U1206
Univ Lyon, INSA-Lyon,
Université Claude Bernard Lyon 1,
UJM-Saint Etienne, CNRS, Inserm
F-69100, Villeurbanne, France
Barbara.Nicolas@creatis.insa-lyon.fr

***Abstract*—Ultrasound Localisation Microscopy (ULM) is an imaging framework which consists of following ultrasound contrast agents, microbubbles, in time, on ultrasound images. The three main steps of ULM are: detecting microbubbles by reducing tissue signal, localizing them with subwavelength precision and tracking their trajectories. ULM performances were evaluated in different studies throughout metrics such as localisation accuracy or capacity to filter the tissues. In parallel, adaptive beamforming offers narrower Point Spread Function (PSF) and/or better tissue filtering than delay-and-sum method classically used within ULM. In this paper, the ability of adaptive beamformers to enhance ULM performances is evaluated, with a particular focus on the trade-off between acquisition time and bubble concentration to achieve super-resolution results.**

***Index Terms*—Adaptive beamforming, Ultrasound Super-Resolution**

I. Introduction

ULM is a super-resolution imaging method used to build microvascular map. It has already been applied, for example, on rat [1] and human [2] brain, to study its ability to detect or prevent stroke and to better understand brain diseases such as Alzheimer's and Parkinson's. It can also be used to detect tumors [3] [4] and to evaluate anticancer therapy effects [5] [6]. However, ULM has a limitation due to the trade-off between acquisition time and number of tracked microbubbles (MBs) to map the vascular network. To mitigate this trade-off, this paper explores the possibility of limiting the number of undetected MB based on adaptive beamforming. To sustain the motivation of this work, ULM framework is displayed in Fig. 1a. First, from images beamformed with delay-and-sum (DAS) algorithm tissues are filtered with a Singular Value Decomposition (SVD) [7] to enable MB detection. The step of MB isolation consists in keeping only non-overlapping MBs, requiring to correctly localize their centers. Finally, tracking their trajectories in vessels allows maping the microvascular network. The steps of tissue filtering and MB isolation lead to an information loss as the first one attenuates relatively slow MBs [8] and the second one removes the overlapping MBs [1].

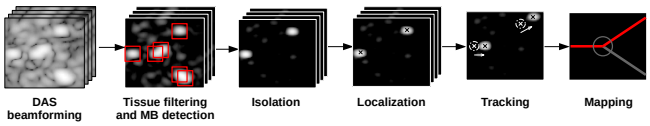

(a) Based on DAS beamforming

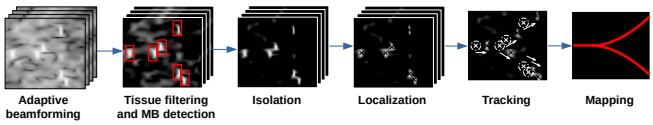

(b) Based on adaptive beamforming

Fig. 1: ULM framework

Consequently, the choice of the beamforming method could have an important impact on the rest of the ULM framework. For example, it is well-known that adaptive beamformers such as the minimum variance one, also called Capon beamformer, provide a better resolved Point Spread Function (PSF) [9]. Due to the improved spatial resolution, MBs that naturally overlap on DAS images, could be separated, and the information loss at the isolation step could be reduced, resulting into more complete vessel map reconstruction, as illustrated in Fig. 1b.

Other beamforming algorithms like pDAS [10] and iMAP [11] have been shown to attenuate speckle compared to DAS, representing thus good candidates for ULM. In this paper, the influence of these adaptive beamformers is evaluated on simulated and experimental chicken embryo data.

II. Material and method

A. Simulated and in vivo datasets

The simulated dataset, provided by the Performance Assessment of Localization Algorithms (PALA) toolbox[1] [12], corresponds to moving MBs at various velocities and trajectories. The simulation main parameters are given in Tab. I. To enhance the simulation realism, an immobile residual speckle has been added. The ground truth of the MBs positions is available in the toolbox to evaluate detection metrics such as True Positive (TP), False Negative (FN) and False Positive (FP).

The *in vivo* dataset has been acquired on a chicken embryo with a Verasonics linear probe in plane wave mode. A specific area with bifurcations, which is interesting in the case of ULM, is chosen. Parameters of acquisition and beamforming are given in Tab. I.

TABLE I: Acquisition parameters for each dataset

Parameter	Simulated dataset	*In vivo* dataset
US frequency	7.8MHz	7.8MHz
Wavelength λ	197μm	197μm
Pixel size	$\lambda/2$	$\lambda/2$
Framerate	500Hz	400Hz
Acquisition time	40s	60s

B. Beamforming methods

During the acquisition, the emitted plane wave is returned as echoes by scatterers in the environment to image. The first step is to rephase each received echo to isolate the energy along the corresponding backscattered wave. According to the DAS, the second step is to sum the rephased signals, with an eventual weighting vector, to get the corresponding pixel intensity [13]. Adaptive beamforming processes in the same way except for the weighting, which is adaptive and computed from the rephased signals. In this paper, in addition to DAS, three different beamformers are studied in the context of ULM.

- The Capon beamforming [14] [15] computes a weighting vector that minimizes the variance of the rephased signal to attenuate eventual disturbing source. In practice, this calculation rule leads to a thinner PSF.
- The pDAS beamforming [10] is a generalization of the FD-MAS beamforming [16]. The weighting vector computation is based on the rephased signal autocorrelation. The motivation is to isolate the constant component whose autocorrelation is higher than noise or speckle component. A parameter p defines the autocorrelation order. In the following, the method is referred to as 2pDAS for $p = 2$ and 3pDAS for $p = 3$.
- The iMAP beamformer [11] considers the rephased signals as the sum of the constant backscattered amplitude and a random noise supposed Gaussian. The objective is to find the mean and the standard deviation of the theoretical Gaussian distribution that maximizes its resemblance with the values of the rephased vector. The effect of this beamformer is thus to increase the constant component relatively to the noise level. In practice, to estimate the Gaussian mean and variance, the algorithm is iterative but only 1 or 2 iterations are enough to obtain good results. In the following, this method is denoted as 1iMAP for 1 iteration and as 2iMAP for 2 iterations.

[1]available at https://zenodo.org/record/4343435

C. Ultrasound Localization Microscopy method

The algorithm used to perform ULM is the one provided in the PALA toolbox. The localization method chosen is based on the radial symmetry [17], since it presents a good ratio between performance and computational cost.

The values of the hyperparameters are given in Table II. For the *in vivo* dataset, the SVD threshold was chosen by identifying tissue, MB and noise curve pattern on the singular values distribution as explained in [18].

TABLE II: ULM hyperparameters for each dataset

Parameter	Simulated dataset	*In vivo* dataset
ROI size	3 pixels	3 pixels
Number of particles to detect	40 per frame	20 per frame
SVD cutoff	No SVD	3
Max linking distance	2	1
Minimum track length	15	20
Density map resolution	$\lambda/10$	$\lambda/10$

III. Results and discussion

A. Results on simulated dataset

The raw data resulting from this simulation have been used to reconstruct the images using the different beamformers introduced in the previous section. One image resulting from each beamformer is plotted in Fig. 2, highlighting the characteristics and in particular the potential benefits for ULM of each algorithm.

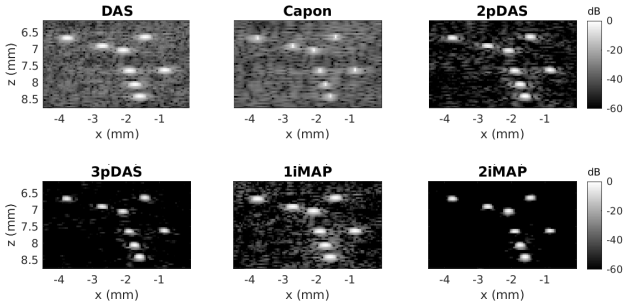

Fig. 2: Simulated image beamformed with the different beamformers considered (zoom on MBs)

Due to the available ground truth, it is possible to count the detected MBs (TP), missed ones (FN) and the false alarm (FP). A TP is counted if a MB is detected by the algorithm in a radius of $\lambda/4$ around the ground truth and a FN is counted if there is no detection in this range. The FP corresponds to detections where there is no simulated MB at a distance of $\lambda/4$. Fig. 3 regroups the three metrics for each beamformer. One can see that Capon and 2iMAP allow to detect around $85,000$ more MBs and $50,000$ less false alarm compared to DAS. The pDAS beamformer also helps to detect more MBs, at the cost of more false alarm compared to DAS. This is due to high side-lobes on pDAS images, as it can be seen in Fig. 2, which turn into false MB detections. The 3pDAS beamformer attenuates these side-lobes and thus decreases these errors. Finally, the 1iMAP is only slightly better than DAS, which can be explained by the fact that its iterative process is initalized by DAS.

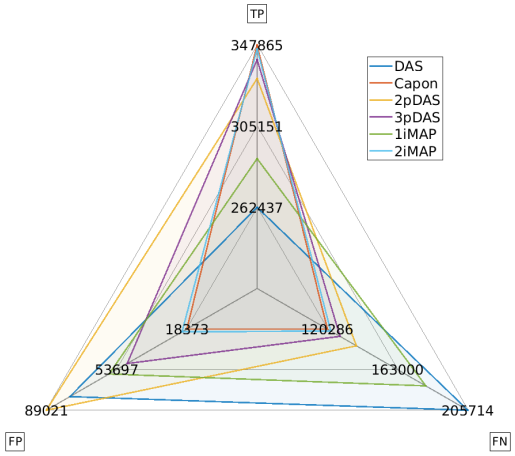

Fig. 3: Detection metrics for each beamformer

This improved MB detections performance due to adaptive beamformers, in particular Capon and 2iMAP, can be explained by two linked phenomenon. The first one is a better spatial resolution in the lateral and axial directions, due to a thinner PSF. Indeed, it can be seen in Fig. 4 that the distance between localized MBs and ground truth present a thinner distributions, especially for the 2iMAP beamformer, in both lateral and axial directions. The second one is the ability to separate MBs that are overlapped with the DAS. This can be seen in Fig. 5 where the adaptive beamformers (except 1iMAP, for the reason mentioned above) allow an accurate reconstruction of the bifurcation thanks to more individual PSF detected.

B. Results on in vivo

Fig. 6 shows US images of a specific area of chicken embryo with injected microbubbles, highlighting the benefits of adaptive beamforming on experimental data.

The results in Fig. 7 show that Capon is equivalent to DAS. However, pDAS and iMAP allow slow bubble detection in chicken embryo experiment. In particular, one can see bright

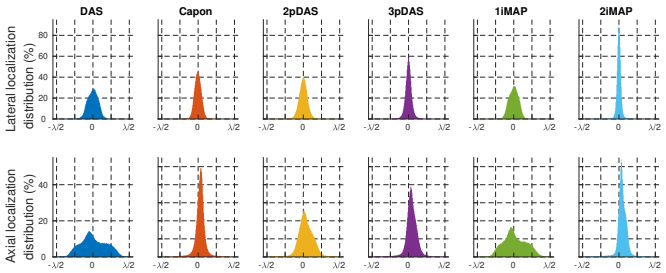

Fig. 4: MB localization error distribution for each beamformer

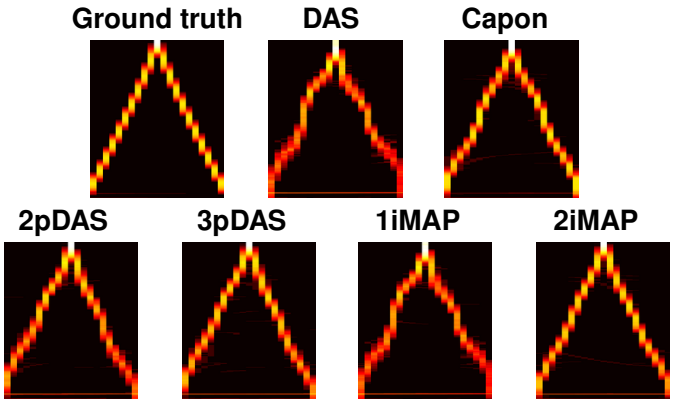

Fig. 5: Specific area of vertical branches with a maximum gap of 2λ, beamformed with each beamformer. All images are normalized by the maximum value of the DAS result.

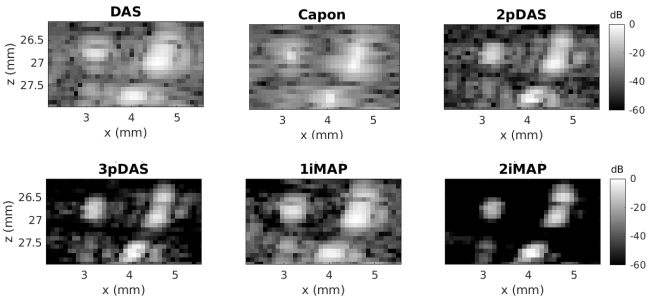

Fig. 6: Chicken embryo data beamformed with several beamformers (zoom on MBs) after SVD filtering

areas with pDAS and iMAP, which correspond to vessels perpendicular to the imaging plane. From the ultrasound probe perspective, these bubbles are almost stationary. This is due to tissue filtering based on SVD that attenuates slow MBs. The pDAS and iMAP beamformers help to increase the relative intensity of these MBs to make them still detectable even after SVD filtering. This represents an important advantage to reconstruct capillaries (e.g., in tumors) with ULM, where bubbles are relatively slow. However, the adaptive beamformers present missed detections on *in vivo* data. Thus, in that case, the adaptive beamforming allows to build a complementary ULM map with slow MBs but not a more complete one.

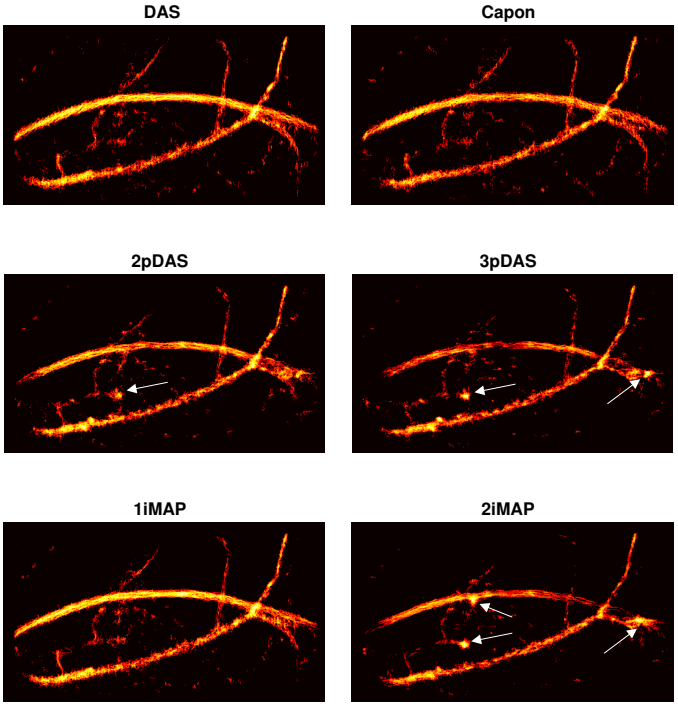

Fig. 7: MB density map on chicken embryo data. All images are normalized by the maximum value of the DAS result.

IV. Conclusion

In this paper, it has been demonstrated through a simulation study that adaptive beamforming allows to detect more individual MBs and to localize them more precisely in both axial and lateral directions. The main consequence is a better reconstruction of a bifurcation.

Furthermore, the influence of adaptive beamforming in ULM is studied on an *in vivo* dataset of chicken embryo. This result highlighted the fact that the adaptive beamformers best filtering the tissues allow to detect slow MBs, which is very important as they are usually strongly attenuated by the tissue filtering. However, there is no significant difference between DAS and Capon in the experimental study. A further work to highlight the benefits of Capon would be to apply it on high concentration data with bifurcations to evaluate the trade-off between MB concentration and acquisition time.

Acknowledgments

This work was supported by the LABEX CELYA (ANR-10-LABX-0060) and LABEX PRIMES (ANR-11-LABX-0063) of Université de Lyon, within the program "Investissements d'Avenir" (ANR-11-IDEX-0007) operated by the French National Research Agency (ANR). We would like to acknowledge the authors of the PALA toolbox for having made publicly available the ULM Matlab codes and ultrasound datasets.

References

[1] O. Couture, V. Hingot, B. Heiles, P. Muleki-Seya, and M. Tanter, "Ultrasound Localization Microscopy and Super-Resolution: A State of the Art," *IEEE Transactions on Ultrasonics, Ferroelectrics and Frequency Control*, vol. 65, no. 8, pp. 1304–1320, Aug. 2018. [Online]. Available: https://hal.archives-ouvertes.fr/hal-02344318

[2] C. Demené, J. Robin, A. Dizeux, B. Heiles, M. Pernot, M. Tanter, and F. Perren, "Transcranial ultrafast ultrasound localization microscopy of brain vasculature in patients," *Nature Biomedical Engineering*, vol. 5, no. 3, pp. 219–228, 2021. [Online]. Available: http://dx.doi.org/10.1038/s41551-021-00697-x

[3] F. Lin, J. D. Rojas, and P. A. Dayton, "Super resolution contrast ultrasound imaging: Analysis of imaging resolution and application to imaging tumor angiogenesis," in *2016 IEEE International Ultrasonics Symposium (IUS)*, 2016, pp. 1–4.

[4] F. Lin, S. Shelton, D. Espindola, J. Rojas, G. Pinton, and P. Dayton, "3-d ultrasound localization microscopy for identifying microvascular morphology features of tumor angiogenesis at a resolution beyond the diffraction limit of conventional ultrasound," *Theranostics*, vol. 7, pp. 196–204, 01 2017.

[5] T. Opacic, S. Dencks, B. Theek, M. Schulte, D. Ackermann, A. Rix, T. Lammers, E. Stickeler, S. Delorme, G. Schmitz, and F. Kiessling, "Motion model ultrasound localization microscopy for preclinical and clinical multiparametric tumor characterization," *Nature Communications*, vol. 9, 04 2018.

[6] D. Ghosh, F. Xiong, R. Mattrey, S. Sirsi, and K. Hoyt, "Monitoring early tumor response to vascular targeted therapy using super-resolution ultrasound imaging," in *2017 IEEE International Ultrasonics Symposium (IUS)*, 2017, pp. 1–1.

[7] C. Demené, T. Deffieux, M. Pernot, B. F. Osmanski, V. Biran, J. L. Gennisson, L. A. Sieu, A. Bergel, S. Franqui, J. M. Correas, I. Cohen, O. Baud, and M. Tanter, "Spatiotemporal Clutter Filtering of Ultrafast Ultrasound Data Highly Increases Doppler and fUltrasound Sensitivity," *IEEE Transactions on Medical Imaging*, vol. 34, no. 11, pp. 2271–2285, 2015.

[8] J. Brown, K. Christensen-Jeffries, S. Harput, G. Zhang, J. Zhu, C. Dunsby, M.-X. Tang, and R. J. Eckersley, "Investigation of microbubble detection methods for super-resolution imaging of microvasculature," *IEEE Transactions on Ultrasonics, Ferroelectrics, and Frequency Control*, vol. 66, no. 4, pp. 676–691, 2019.

[9] B. M. Asl and A. Mahloojifar, "Contrast enhancement and robustness improvement of adaptive ultrasound imaging using forward-backward minimum variance beamforming," *IEEE Transactions on Ultrasonics, Ferroelectrics, and Frequency Control*, vol. 58, no. 4, pp. 858–867, 2011.

[10] M. Polichetti, F. Varray, J.-C. Béra, C. Cachard, and B. Nicolas, "A nonlinear beamformer based on p-th root compression—application to plane wave ultrasound imaging," *Applied Sciences*, vol. 8, no. 4, 2018. [Online]. Available: https://www.mdpi.com/2076-3417/8/4/599

[11] T. Chernyakova, D. Cohen, M. Shoham, and Y. C. Eldar, "IMAP Beamforming for High-Quality High Frame Rate Imaging," *IEEE Transactions on Ultrasonics, Ferroelectrics, and Frequency Control*, vol. 66, no. 12, pp. 1830–1844, 2019.

[12] B. Heiles, A. Chavignon, V. Hingot, P. Lopez, E. Teston, and O. Couture, "Performance benchmarking of microbubble-localization algorithms for ultrasound localization microscopy." *Nat Biomed Eng*, 2022. [Online]. Available: https://doi.org/10.1038/s41551-021-00824-8

[13] V. Perrot, M. Polichetti, F. Varray, and D. Garcia, "So you think you can das? a viewpoint on delay-and-sum beamforming," *Ultrasonics, Elsevier*, vol. 111, p. 106309, 2021. [Online]. Available: https://www.sciencedirect.com/science/article/pii/S0041624X20302444

[14] P. Stoica and R. Moses, *Spectral Analysis of Signals*, 2005.

[15] J. F. Synnevåg, A. Austeng, and S. Holm, "Benefits of minimum-variance beamforming in medical ultrasound imaging," *IEEE Transactions on Ultrasonics, Ferroelectrics, and Frequency Control*, vol. 56, no. 9, pp. 1868–1879, 2009.

[16] G. Matrone, A. S. Savoia, and G. Magenes, "Filtered delay multiply and sum beamforming in plane-wave ultrasound imaging: Tests on simulated and experimental data," pp. 1–4, 2016.

[17] R. Parthasarathy, "Rapid, accurate particle tracking by calculation of radial symmetry centers," *Nature Methods*, vol. 9, no. 7, pp. 724–726, 2012.

[18] J. Baranger, B. Arnal, F. Perren, O. Baud, M. Tanter, and C. Demene, "Adaptive Spatiotemporal SVD Clutter Filtering for Ultrafast Doppler Imaging Using Similarity of Spatial Singular Vectors," *IEEE Transactions on Medical Imaging*, vol. 37, no. 7, pp. 1574–1586, 2018.